Photosynth Res (2016) 129:43–58
DOI 10.1007/s11120-016-0262-x

ORIGINAL ARTICLE

A novel mechanistic interpretation of instantaneous temperature responses of leaf net photosynthesis

Jörg Kruse[1] · Saleh Alfarraj[2] · Heinz Rennenberg[1,2] · Mark Adams[3]

Received: 2 October 2015 / Accepted: 11 April 2016 / Published online: 24 May 2016

Abstract Steady-state rates of leaf CO_2 assimilation (A) in response to incubation temperature (T) are often symmetrical around an optimum temperature. A/T curves of C_3 plants can thus be fitted to a modified Arrhenius equation, where the activation energy of A close to a low reference temperature is strongly correlated with the dynamic change of activation energy to increasing incubation temperature. We tested how $[CO_2] <$ current atmospheric levels and saturating light, or $[CO_2]$ at 800 µmol mol^{-1} and variable light affect parameters that describe A/T curves, and how these parameters are related to known properties of temperature-dependent thylakoid electron transport. Variation of light intensity and substomatal $[CO_2]$ had no influence on the symmetry of A/T curves, but significantly affected their breadth. Thermodynamic and kinetic (physiological) factors responsible for (i) the curvature in Arrhenius plots and (ii) the correlation between parameters of a modified Arrhenius equation are discussed. We argue that the shape of A/T curves cannot satisfactorily be explained via classical concepts assuming temperature-dependent shifts between rate-limiting processes. Instead the present results indicate that any given A/T curve appears to reflect a distinct flux mode, set by the balance between linear and cyclic electron transport, and emerging from the anabolic demand for ATP relative to that for NADPH.

Keywords Temperature response · Non-linear Arrhenius plot · Cyclic electron flow · Photorespiration

Abbreviations

A_{ref}	Net photosynthesis at the reference temperature
A_{opt}	Peak rates of net photosynthesis at optimum temperature
T_{ref}	Low reference temperature (294 K in the present study)
T_{opt}	Optimum temperature
E_{oA}	Activation energy of A at some (unspecified) incubation temperature
$E_o(\mathrm{Ref}_A)$	Activation energy of A infinitesimally close to (or 'at') the reference temperature
δ_A	Dynamic response of E_{oA} to changes in incubation temperature
ETR	Linear electron transport rate
$E_o(\mathrm{Ref}_{ETR})$	Activation energy of ETR at the reference temperature
δ_{ETR}	Dynamic response of E_{oETR} to changes in incubation temperature
c_a	Applied CO_2 concentration during measurements
c_i	Intercellular $[CO_2]$, Φ_{PSII}, photochemical efficiency of PS II of light-adapted leaves ('operating efficiency')
CEF	Cyclic electron flow around PS I

Electronic supplementary material The online version of this article (doi:10.1007/s11120-016-0262-x) contains supplementary material, which is available to authorized users.

✉ Jörg Kruse
joerg.kruse@ctp.uni-freiburg.de

[1] Chair of Tree Physiology, Institute of Forest Sciences, Georges-Köhler-Allee 53/54, 79110 Freiburg, Germany

[2] College of Sciences, King Saud University, P.O. Box 2455, Riyadh 11451, Saudi Arabia

[3] Faculty of Agriculture and Environment, The University of Sydney, Sydney, NSW 2006, Australia

Introduction

The instantaneous temperature response of leaf CO_2 assimilation (A) measured under ambient atmospheric CO_2 and stable light interception can be described by a bell-shaped optimum curve, provided that sufficient time is given to allow Calvin cycle activity to equilibrate to respective incubation temperatures (T) (Berry and Björkman 1980; Battaglia et al. 1996). In the face of climate change and expected temperature increases within the twenty-first century, there is renewed interest in instantaneous A/T responses and the information that can be obtained thereof (Smith and Dukes 2013). A/T responses are a viable tool to probe a species' acclimation potential to growth temperature alteration (Way and Yamori 2014; see companion study Kruse et al. 2016). However, we presently lack a comprehensive mechanistic understanding of the processes that cause variation in the shape of observed temperature responses. Declining rates of net photosynthesis above the optimum temperature (T_{opt}), for example, have traditionally been interpreted in terms of shifts between rate-limiting processes, i.e., between the rate of carboxylation (A_C) and that of ribulose bisphosphate regeneration (A_J)(Farquhar et al. 1980). To date, it has not been possible to unequivocally identify the process that limits net photosynthesis above T_{opt} (see references in Kruse et al. 2016). The notional concept that distinguishes between two (or three, if triosephosphate utilization is included) potential biochemical limitations is well suited to interpret the response of A to intercellular CO_2 availability (c_i), and to infer fundamental information about the biochemical capacity of C_3 photosynthesis (i.e., V_{cmax} and J_{max}), but may not help advance our mechanistic understanding of photosynthetic temperature responses. This is partly because identification of putative biochemical limitations of A across a range of incubation temperatures can be confounded by diffusional limitations, i.e., restricted CO_2 transfer to chloroplasts (Lin et al. 2012). It is probably for these reasons that measurements of A/c_i responses are much more common than those of A/T responses. Nonetheless, we recently showed that application of a modified Arrhenius equation can help further elucidation of physiological mechanisms underlying photosynthetic temperature responses (Kruse et al. 2016).

Data obtained via A/T responses can be fitted to a modified Arrhenius equation, provided incubation temperatures do not exceed those to which plants are acclimated or adapted (Kruse et al. 2016):

$$\ln A = \ln A_{ref} + \frac{E_o(\mathrm{Ref}_A)}{\Re} \times \frac{T - T_{ref}}{T \times T_{ref}} + \delta_A \times \left(\frac{T - T_{ref}}{T \times T_{ref}}\right)^2, \quad (1)$$

where $\ln A$ is the logarithmic rate of CO_2 assimilation (μmol m^{-2} s^{-1}), T is the incubation temperature (K), $\Re$ is the universal gas constant, $\ln A_{ref}$ is the (logarithmic) assimilation rate at the reference temperature (T_{ref}), E_o (Ref_A) is the activation energy of CO_2 assimilation close to the reference temperature (kJ mol^{-1}), and δ_A (kK^2) describes the temperature sensitivity of E_{oA}.

Temperature responses of steady-state rates of CO_2 assimilation have noteworthy features. First, activation energy of overall net CO_2 assimilation (i.e., E_{oA}) within any (infinitesimally small) temperature interval of the A/T curve can be derived as:

$$\frac{dy}{dx} = \frac{E_o(\mathrm{Ref}_A)}{\Re} + 2\delta_A \times x, \quad (2)$$

where $y = \ln A$ and $x = \frac{T - T_{ref}}{T \times T_{ref}}$ (see Eq. 1). Individual A/T curves greatly vary and can either be rather flat (with little temperature sensitivity of E_{oA} or small δ_A), or show pronounced curvature (or large δ_A)—depending on species and growth conditions (i.e., Yamori et al. 2005, Gunderson et al. 2010, von Caemmerer and Evans 2015). Strikingly, parameter values for $E_o(\mathrm{Ref}_A)$ and δ_A (see Eq. 2), obtained from a large diversity of A/T curves, are strongly correlated (Kruse et al. 2016).

A second feature of A/T curves is related to their apparent symmetry:

$$\frac{d^2y}{dx^2} = 2 \times \delta_A = \text{constant} \quad (3)$$

For any individual A/T curve, the decline of E_{oA} with increasing T is constant (Kruse et al. 2016). A/T curves do not show an inflection point within the range of 'moderate' incubation temperatures (e.g., between 15 and 40 °C). Temperature-dependent increases in steady-state rates of CO_2 assimilation up to a thermal optimum (T_{opt}), are similar in most respects to the decline above T_{opt}. This is a rather surprising result, since increased leaf temperature is usually argued to increase rates of photorespiration. The affinity of Rubisco for CO_2 and O_2 also changes with temperature, favoring oxygenation of Ribulose-1,5-P_2 at greater T (Berry and Björkman 1980; Harley et al. 1985). Additionally, temperature-dependent changes in solubility of gaseous substrates might, at greater T, decrease the availability of CO_2 relative to that of O_2 at the active site of Rubisco (Siedow and Day 2000).

Despite these temperature-dependent processes, symmetric responses to changing incubation temperature have also been reported for thylakoid electron transport. June et al. (2004) estimated the temperature dependency of linear electron transport from that of PSII quantum yield (Φ_{PSII}) via fluorescence measurements. They conducted measurements at 1250 ppm CO_2, in order to minimize photorespiration and limitation of A by Rubisco activity,

and 1200 μmol quanta m^{-2} s^{-1}. Temperature scans of Φ_{PSII} can be obtained quickly, taking about 20–25 min to cover a temperature range from 15 to 43 °C. The temperature response of electron transport in intact soybean leaves could be described as (June et al. 2004):

$$J(T_L) = J(T_O) \times e^{-\left(\frac{T_L - T_O}{\Omega}\right)^2}, \quad (4)$$

where T_L is the leaf temperature (°C), $J(T_o)$ is the rate of electron transport at the optimum temperature T_o, and Ω is the difference in temperature from T_o at which J falls to e^{-1} (=0.37) of its value at T_o. This equation describes a range of temperature dependencies of J, as reported in the literature (see references in June et al. 2004). Equally important, the decline of J above T_{opt} seems fully reversible. Irreversible deactivation of PSII, depends on species and growth conditions, but T 43–45 °C is often described as deleterious for plants on this basis (Seemann et al. 1984; Zhang and Sharkey 2009; Hüve et al. 2011).

In the present study, we analyzed the temperature dependencies of steady-state CO_2 assimilation and thylakoid electron transport between 22 and 41 °C leaf temperature of Date palm (*Phoenix dactylifera*). Our first objective was to test if measurements conducted at saturating light and $c_a <$ ambient (between 380 and 80 μmol mol^{-1}), i.e., conditions that should progressively increase photorespiration, changed the symmetry of A/T curves and/or the correlation between $E_o(Ref_A)$ and δ_A. Secondly, in order to assess the influence of light intensity on the parameters that describe the A/T curve, we measured temperature responses at c_a ambient (800 μmol mol^{-1}) and variable light (between 20 and 1500 μmol quanta m^{-2} s^{-1}), i.e., conditions that tend to limit A via electron transport at low irradiance or via limited capacity of Ribulose-1,5-P_2 regeneration at high irradiance. Our second set of experiments was augmented with measurements of temperature-dependent electron transport (fitted with Eq. 1), in order to compare parameters of A/T curves with those obtained for thylakoid electron transport. Our general aim was to elucidate regulation of CO_2 assimilation under steady-state conditions.

Materials and methods

Plant material and growth conditions

Two-year-old seedlings of Date palm (*Phoenix dactilyfera*) were purchased from a commercial supplier ('Der Palmenmann', Bottrop, Germany). Eight or eleven months before the start of respective experiments, plants were repotted (2 liter pots; peat–sand–perlite mixture, 20:30:50 (vol%); 15 g of NPK fertilizer per pot), grown under greenhouse conditions (15–25 °C, 60–70 % rH) and irrigated twice per week (*c*. 500 ml per pot). The two sets of experiments were conducted in January and April 2014, respectively, using different sets of plant material. For each experiment, five plants were transferred from the greenhouse to a climate-controlled growth chamber (Heraeus, Vötsch, Germany). Growth temperature was set at 25 °C during the light period and 20 °C during the dark period (16/8 h), and incident light reached 200 μmol photons m^{-2} s^{-1} at leaf level. Plants were given 2 weeks' time to acclimate to growth conditions in the chamber prior to gas exchange measurements, and continued to be irrigated twice per week throughout the experiments.

Gas exchange and fluorescence measurements

Temperature responses of CO_2 assimilation were determined via a portable gas exchange measuring system, equipped with a LED light source combined with PAM chlorophyll fluorometer (GFS 3000, Walz, Effeltrich, Germany). Palm leaves were placed into the 8 cm^2 cuvette of the system that was flushed with air at a defined flow rate of 700 μmol s^{-1} (13,000 ppm H_2O in incoming air). Temperature responses were determined in seven 3 °C steps, ranging from 21 to 39 °C cuvette temperature (accuracy ±0.1 °C). Leaf temperature was determined via a thermocouple touching the lower leaf surface (accuracy ±0.2 °C), and was 1.3–2.4° greater than surrounding air temperature, depending on applied [CO_2] (c_a) or incident light (photosynthetic photon flux density, PPFD). At the reference temperature (T_{ref} = 294 K or 21 °C), leaves were allowed 20 min to equilibrate, before gas exchange was recorded and averaged over a period of 5 min. After each subsequent temperature change, plants were given 10 min until steady-state conditions were attained, prior to recording the 5 min average of gas exchange rates. Hence, determination of each individual A/T curve took 2 h (first set of experiments), or 2 h 15 min (second set of experiments).

In the first set of experiments, temperature responses were recorded at saturating light intensity (1200 μmol quanta m^{-2} s^{-1}), and CO_2 concentrations of incoming air that varied from 80 to 380 μmol mol^{-1}. In the second set of experiments, temperature responses were recorded at c_a = 800 μmol mol^{-1} (incoming air), and stable light intensities varied from 20 to 1500 μmol quanta m^{-2} s^{-1}. After stabilization and recording of gas exchange, a pulse of saturating light was applied (4500 μmol m^{-2} s^{-1}), to fully reduce PSII. The fluorescence signals before and during each flash were detected via PIN photodiode protected by long-pass filter (>660 nm) (Walz, Effeltrich, Germany). Photochemical efficiency of PS II (Φ_{PSII}) of

light-adapted leaves ('operating efficiency') was determined according to Genty et al. (1989):

$$\phi_{PSII} = \left(F'_m - F'\right)/F'_m, \quad (5)$$

where F'_m is the maximum fluorescence level caused by the saturating light flash and F' is the steady-state fluorescence from the light-adapted leaf.

Rates of linear electron transport (ETR) were estimated as (Schreiber 2004):

$$J = \phi_{PSII} \times \alpha \times 0.5 \times PPFD, \quad (6)$$

where α is the total leaf absorbance (assumed to be 0.84; Baker et al. 2007), and the factor 0.5 describes the expected distribution of light between the two photosystems. We note, however, that extended exposure to greater temperature (i.e., 30 min) may reduce the fraction of light utilized by PSII (Zhang and Sharkey 2009).

Responses of *A* and *ETR* to leaf temperature were fitted with Eq. 1, in order to obtain respective parameter values. Optimum temperatures of *A* and *ETR* were calculated from the first derivative of Eq. 1 (i.e., according to Eq. 2; compare Kruse et al. 2016). C_i at T_{opt} and Φ_{PSII} at T_{opt} were derived via interpolation between data points enclosing T_{opt}.

Statistical analysis

Statistical analysis was performed with 38–40 temperature response curves per experiment. In order to analyze the effects of c_i (at T_{opt}), on the correlation between $E_o(\mathrm{Ref}_A)$ and δ_A, data were subjected to a General Linear Model (GLMs; STATISTCA, version 10.0, StatSoft, Inc, Tulsa, OK, USA). Effect sizes of c_i at T_{opt} (factor1) and $E_o(\mathrm{Ref}_A)$ (factor 2) on the dependent variable, i.e., δ_A, were estimated from partial η^2:

$${}_p\eta^2 = \frac{SS_{factor}}{SS_{factor} + SS_{residual}} \quad (7)$$

In analogous fashion, we tested the influences of light intensity (factor 1) and $E_o(\mathrm{Ref}_A)$ (factor 2) on δ_A; the influence of light intensity and $E_o(\mathrm{Ref}_{ETR})$ on δ_{ETR}; and the influences of light intensity and δ_{ETR} on δ_A.

Results

Gas exchange characteristics

Effects of variable c_a (at fixed light intensity) and variable light (at fixed c_a) on the temperature response of CO_2 assimilation are characterized by significant differences in stomatal behavior. At variable $c_a <$ ambient, the temperature dependency of stomatal conductance (g_s) followed a bell-shaped optimum curve (Fig. 1a). Peak rates of g_s and the curvature of the response varied with applied c_a (hence the large standard deviation in Fig. 1a). Conversely, the temperature response of c_i was comparatively stable at variable c_a (Fig. 1b). Application of 800 µmol mol^{-1} CO_2 at variable light and fixed c_a led to stomatal closure. Averaged across different light intensities, stomatal conductance at 800 µmol mol^{-1} showed little variation with leaf temperature (Fig. 1a). However, c_i steadily declined from 560 µmol mol^{-1} at ~23 °C to 380 µmol mol^{-1} at ~41 °C (Fig. 1b).

There was no evidence for an effect of c_i (determined at T_{opt} of *A*) on the symmetry of *A*/*T* curves (Fig. 1c). At variable $c_a <$ ambient, *A*/*T* curves were well described by Eq. 1, irrespective of c_i (average $R^2 = 0.98$). The second set of experiments produced similar results ($R^2 = 0.93$). While some individual data points deviated from the line of best fit, there was no evidence of biological significance of that variation (sensu Kubo 1985). There was no systematic or re-occurring deviation at any given incubation temperature.

In the second set of experiments, photosynthetic efficiency of PSII was recorded in parallel to gas exchange. Φ_{PSII} at T_{opt} of *A* declined from 0.65 at low light intensity to 0.1 at saturating light, similar to previous reports (Clarke and Johnson 2001; Hald et al. 2008).

Effects of c_i and light intensity on parameters of the *A*/*T* response curve

Within the CO_2-limited range of assimilation, A_{opt} (determined at T_{opt}) increased linearly with c_i (determined at T_{opt}). This correlation explained 65 % of the observed variation. Much of the residual variation is likely explained by differences in V_{cmax} between different leaves (Fig. 2a). The symmetry of *A*/*T* curves (i.e., δ_A) was apparently unrelated to c_i at T_{opt} (Fig. 2b). $E_o(\mathrm{Ref}_A)$ and δ_A were strongly correlated ($R^2 = 0.83$; Fig. 2c).

At variable light and fixed c_a, ETR at T_{opt} (i.e., ETR_{opt}) increased hyperbolically with increasing light intensity (Fig. 2d), as reported elsewhere (Tenhunen et al. 1976; Thornley and Johnson 1990). Light intensity had a significant effect on δ_{ETR}. At low light intensities (and low ETR_{opt}), ETR temperature responses showed little curvature. Curvature became more pronounced as light intensity increased (Fig. 2e). $E_o(\mathrm{Ref}_{ETR})$ and δ_{ETR} were highly correlated, based on interpreted pairs of parameters obtained from measurements of different leaves of different plants ($R^2 = 0.95$; Fig. 2f).

Effects of light intensity on parameters derived from the *A*/*T* curve were similar to those on parameters of temperature-dependent electron transport (Fig. 2g–i). A major difference was that high light intensity caused a much stronger reduction in δ_A than in δ_{ETR} (Fig. 2h). The

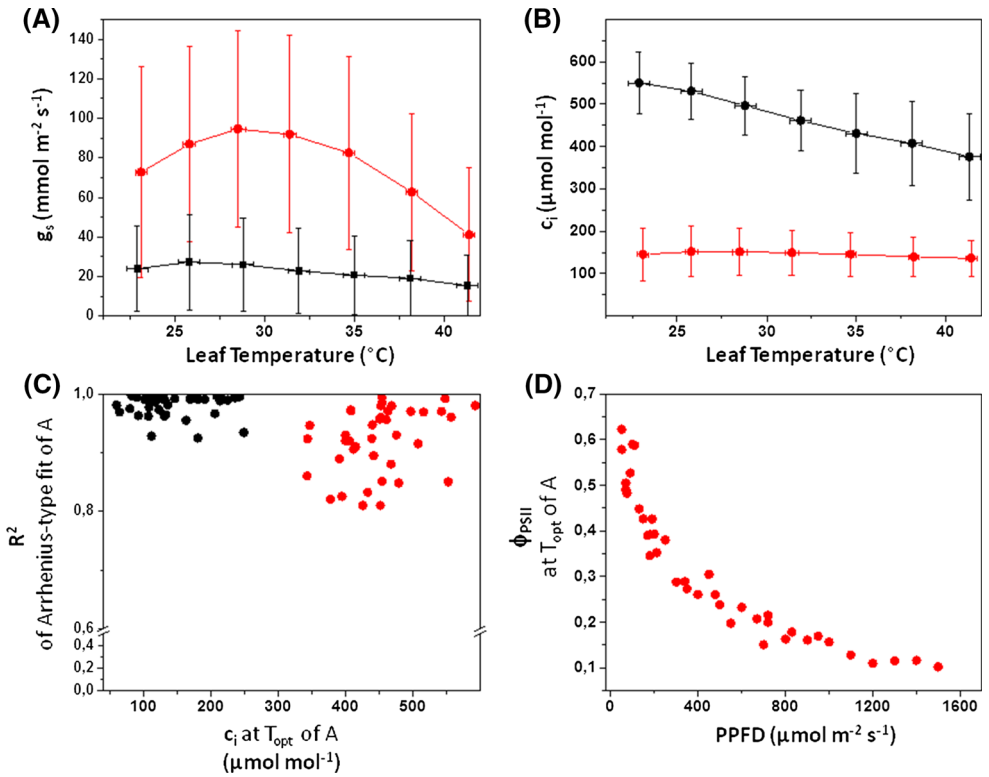

Fig. 1 Gas exchange characteristics of Date Palm trees. In the first set of experiments (black symbols), gas exchange was conducted at variable c_a ambient (80–380 µmol mol^{-1}) and fixed PPFD (1200 µmol quanta m^{-2} s^{-1}). In a second set of experiments (*red symbols*), gas exchange was conducted at fixed c_a ambient (800 µmol mol^{-1}) and variable PPFD (20–1500 µmol quanta m^{-2} s^{-1}). **a** Temperature response of stomatal conductance. **b** Temperature response of substomatal CO_2 concentration (c_i). Data shown in A and B are averages ± SD of 38–40 replicates. **c** Goodness of fit for individual temperature responses of photosynthesis with a 3 parameter, Arrhenius-type equation, plotted against the c_i (at T_{opt} of *A*). **d** Quantum yield of photosystem II (at T_{opt} of *A*), plotted against incident radiation in the second set of experiments (c_a = 800 µmol mol^{-1}) (quantum yield measurements were only available for the second set of experiments)

correlation between E_o(Ref$_A$) and δ_A was less tight ($R^2 = 0.85$; Fig. 2i) than that between E_o(Ref$_{ETR}$) and δ_{ETR} ($R^2 = 0.95$). Slopes and intercepts of correlations between E_o(Ref$_A$) and δ_A depended on light intensity or applied c_a (compare Fig. 2c with i).

The influence of light intensity and c_i on the correlation between E_oA_{Tref} and δA

Additional influences on the correlation between E_o(Ref$_A$) and δ_A were analyzed by GLMs (see "Materials and methods" section). For example, shifts in T_{opt} affect the intercept of the correlation. Light intensity affected neither T_{opt} of *A* nor T_{opt} of ETR (not shown). Light intensity also had no effect on the correlation between E_o(Ref$_{ETR}$) and δ_{ETR} (Fig. 3a, b). However light intensity did affect the correlation between E_o(Ref$_A$) and δ_A (Fig. 3c, d). Separating additional influences of light intensity on δ_A via a GLM (Table 1), revealed a significant impact of light on the slope of the correlation (compare Fig. 2i with Fig. 3d). This effect could be attributed to low Φ_{PSII} under high light (Fig. 4a), while c_i at T_{opt} had no influence on the correlation between E_o(Ref$_A$) and δ_A (Fig. 4b; Table 1). A different picture emerged, when *A*/*T* curves were derived at $c_a <$ ambient. Low c_i (at T_{opt} of *A*) shifted the intercept of the correlation between E_o(Ref$_A$) and δ_A (Fig. 3e, Table 1; compare Fig. 3f with Fig. 2c). Hence, differences in slope and intercept, and 'unexplained' variation in the correlation between E_o(Ref$_A$) and δ_A (Fig. 2c, i), are of significance and were not related to light- or c_i-driven effects on T_{opt}.

The relation between temperature-dependent electron transport and CO_2 assimilation under contrasting light intensity

Optimum temperatures of thylakoid electron transport and CO_2 assimilation were strongly correlated (Fig. 5a), with T_{opt} of ETR being systematically greater by 4–5 °C than T_{opt} of *A*—similar to previous reports (Niinemets et al. 1999; Medlyn et al. 2002). Peak rates of ETR and *A* at respective optimum temperatures were also highly correlated (Fig. 5b). Both temperature responses were

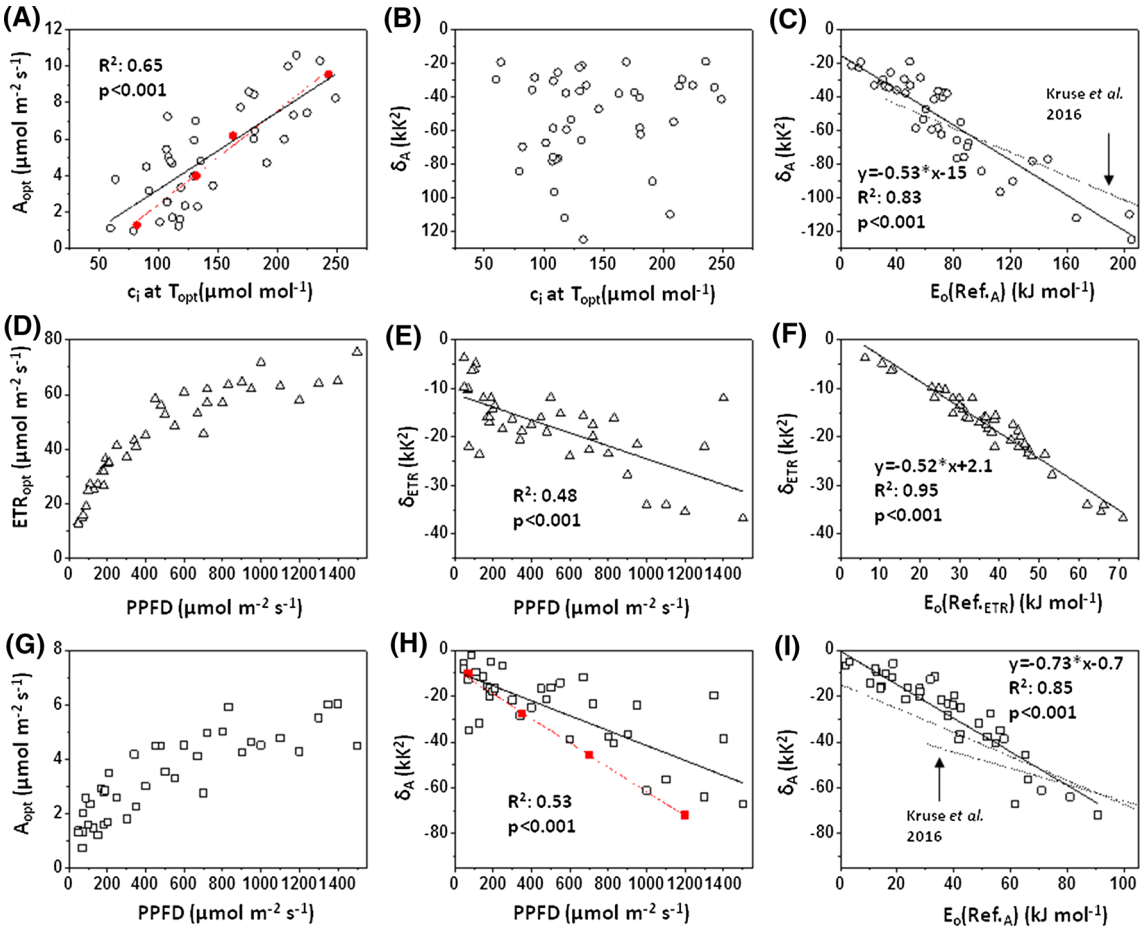

Fig. 2 Relation between model parameters of temperature-dependent photosynthesis or electron transport, and substomatal CO_2 concentration (c_i at T_{opt} of A) or incident light. **a** Correlation between peak rates of photosynthesis achieved at the optimum temperature under saturating light (A_{opt}), and c_i (at T_{opt} of A) within the 'CO_2-limited' range of photosynthesis. The *red data* points were derived from measurements of the same leaf via consecutive measurement of photosynthetic temperature responses at 380, 300, 250, and 120 ppm CO_2. All other data points were derived from independent temperature responses of differing leaves taken from 5 plants. Each temperature curve comprised seven 3 °C steps, ranging from 21 to 39 °C. **b** Temperature sensitivity of E_{oA} (=δ_A) plotted against c_i at T_{opt} of A. **c** Correlation between E_{oA} at the reference temperature (21 °C; $E_o(\mathrm{Ref}_A)$ and δ_A of 'CO_2-limited' photosynthesis. The correlation between these variables derived from an acclimation experiment with Date Palm by Kruse et al. (2016; $T_{ref} = 20$ °C) is drawn for comparison. **d** Hyperbolic relation between electron transport at the optimum temperature (ETR_{opt}) and incident light, measured at $c_a = 800$ µmol mol^{-1}. **e** Correlation between δ_{ETR} and incident light (PPFD). **f** Correlation between $E_o(\mathrm{Ref}_{ETR})$ and δ_{ETR}. **g** Hyperbolic relation between A_{opt} and incident light, measured at $c_a = 800$ - µmol mol^{-1} CO_2. **h** Temperature sensitivity of E_{oA} (=δ_A) plotted against incident light in the second set of experiments ($c_a = 800$ - µmol mol^{-1}). The *red data* points were derived from measurements of the same leaf via consecutive measurement of photosynthetic temperature responses at 1200, 700, 300, and 70 µmol photons m^{-2} s^{-1}. All other data points were derived from independent temperature responses of differing leaves taken from 5 plants. **(I)** Correlation between $E_o(\mathrm{Ref}_A)$ and δ_A of 'light-dependent' photosynthesis. Correlation between these variables derived from 'CO_2-limited' photosynthesis (cf. Figure 2c), and from Kruse et al. 2016 are drawn for comparison. For further statistical analysis of the data compare Figs. 3 and 4, and Table 1

symmetrical, with similar slopes of increase and decrease of ETR or A, below and above respective optimum temperatures. However, the relation between δ_A and δ_{ETR} was subject to other influences and departed strongly from a 1:1 line (Fig. 5c). After accounting for effects of light intensity in a GLM (Table 1), δ_A was 1.5 times greater than δ_{ETR} and the correlation between both variables passed through the origin (zero intercept; compare Fig. 4e with Fig. 5c). Increasing light intensity led to an over-proportional reduction in δ_A (Fig. 4d), i.e., the reduction was stronger for δ_A than for δ_{ETR}.

The activation energy of CO_2 assimilation at fixed reference temperature (294 K or 21 °C in the present study) varied with T_{opt} and δ_A. The correlation between $E_o(\mathrm{Ref}_A)$ and $E_o(\mathrm{Ref}_{ETR})$ showed little deviation from the 1:1 line, because greater δ_{ETR} (as compared to δ_A) was offset by greater T_{opt} of ETR (Fig. 5d). Light intensity had a significant additional effect on the correlation, and explained

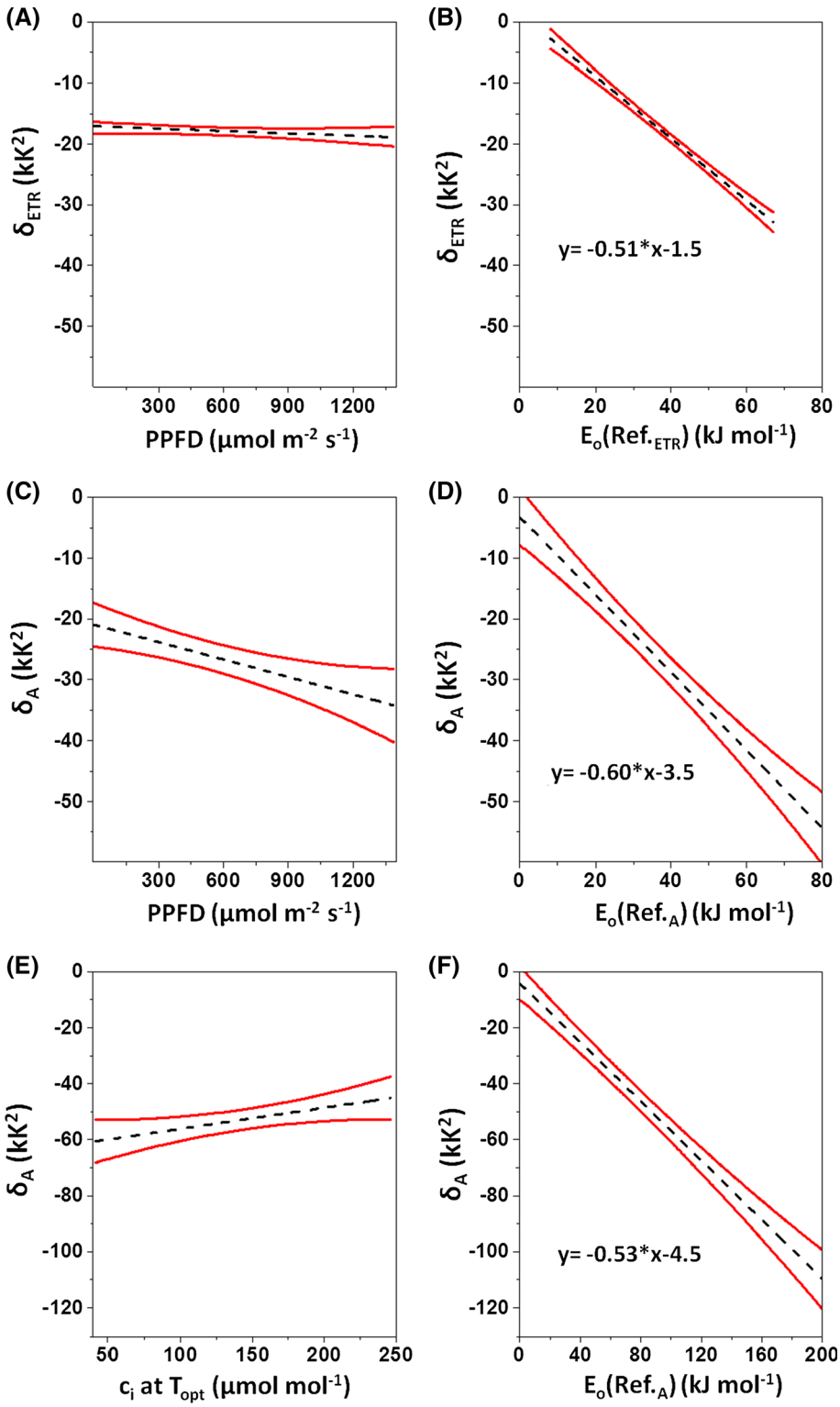

Fig. 3 Correlation between $E_o(\text{Ref}_A)$ (or $E_o(\text{Ref}_{ETR})$) and δ_A (or δ_{ETR}), as affected by incident light and c_i. **a** Effect of incident light on δ_{ETR} (second set of experiments). **b** Correlation between $E_o(\text{Ref}_{ETR})$ and δ_{ETR}, after accounting for effects of incident light (cf. Fig. **a**). Effects predicted by General Linear Models (GLMs) within 95 % confidence intervals are shown. Effects sizes and their significance are shown in Table 1. **c** Effect of incident light on δ_A (second set of experiments). **d** Correlation between $E_o(\text{Ref}_A)$ and δ_A, after accounting for effects of incident light (cf. Fig. **c**). **e** Effect of c_i (at T_{opt} of A) on δ_A (first set of experiments). **f** Correlation between $E_o(\text{Ref}_A)$ and δ_A, after accounting for effects of c_i (cf. Fig. **e**)

Table 1 Results of general linear models (GLMs) testing the influence of incident irradiance and c_i (at T_{opt} of A) on the temperature sensitivity of E_{oA} (=δ_A) or E_{oETR} (=δ_{ETR})

Dependent variable	Independent predictor: ${}_p\eta^2$ (p value)			Entire model: R^2
δ_A	C_i	$E_o(Ref_A)$		Fig. 3a, b
	0.13 (0.02)	**0.85 (<0.001)**		$\boldsymbol{R^2}$ **= 0.90**
δ_A	Light	$E_o(Ref_A)$		Fig. 3c, d
	0.21 (0.004)	**0.74 (<0.001)**		$\boldsymbol{R^2}$ **= 0.91**
δ_{ETR}	Light	$E_o(Ref_{ETR})$		Fig. 3e, f
	0.03 (n.s.)	**0.93 (<0.001)**		$\boldsymbol{R^2}$ **= 0.96**
δ_A	ϕ_{PSII}	C_i	$E_o(Ref_A)$	Fig. 4a, c
	0.18 (0.009)	0.01 (n.s.)	**0.76 (<0.001)**	$\boldsymbol{R^2}$ **= 0.92**
δ_A	Light	δ_{ETR}		Fig. 4d, e
	0.28 (0.009)	**0.56 (<0.001)**		$\boldsymbol{R^2}$ **= 0.83**
$E_o(Ref_A)$	Light	$E_o(Ref_{ETR})$		Not shown
	0.20 (0.007)	**0.38 (<0.001)**		$\boldsymbol{R^2}$ **= 0.73**

Data shown are effect sizes (${}_p\eta^2$) of predictor variables on δ_A and δ_{ETR}. Effects are visualized in Figs. 3 and 4

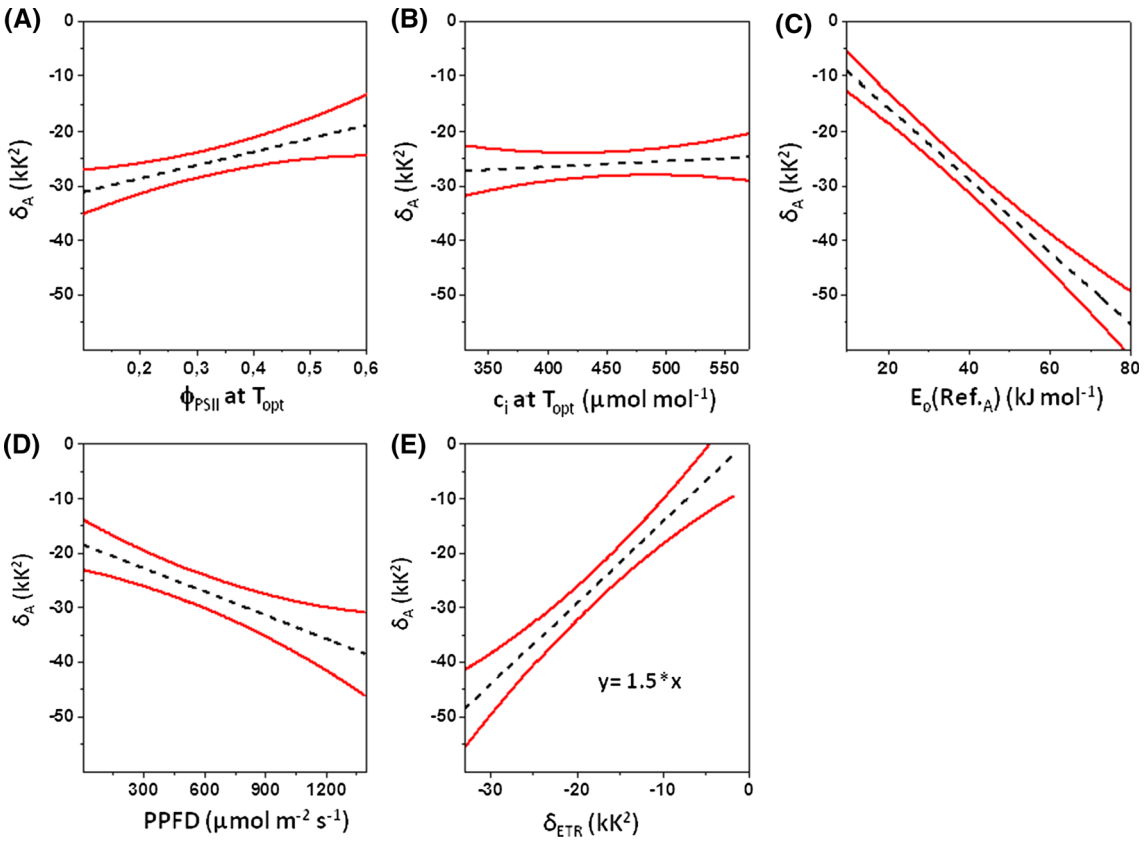

Fig. 4 Correlation between $E_o(Ref_A)$ and δ_A, as affected by c_i and ϕ_{PSII}, or by incident light and δ_{ETR}. **a** Effect of ϕ_{PSII} (at T_{opt} of A) on δ_A (second set of experiments). **b** Effect of c_i (at T_{opt} of A) on δ_A (second set of experiments). **c** Correlation between $E_o(Ref_A)$ and δ_A, after accounting for effects of ϕ_{PSII} and c_i (cf. Fig. **a** + **b**). **d** Effect of incident light on δ_A (second set of experiments). **e** Correlation between δ_A and δ_{ETR}, after accounting for effects of incident light (cf. Fig. **d**). Effects predicted by general linear models (GLMs) within 95 % confidence intervals are shown. Effects sizes and their significance are shown in Table 1

much of the residual variation (73 %, Table 1, as compared to 58 %, Fig. 5d). Some variation is arguably due to fluorescence measurements capturing photosynthetic efficiency of a smaller proportion (e.g., outermost cells) of leaves, while gas exchange provides a more integrated measure of whole-leaf performance.

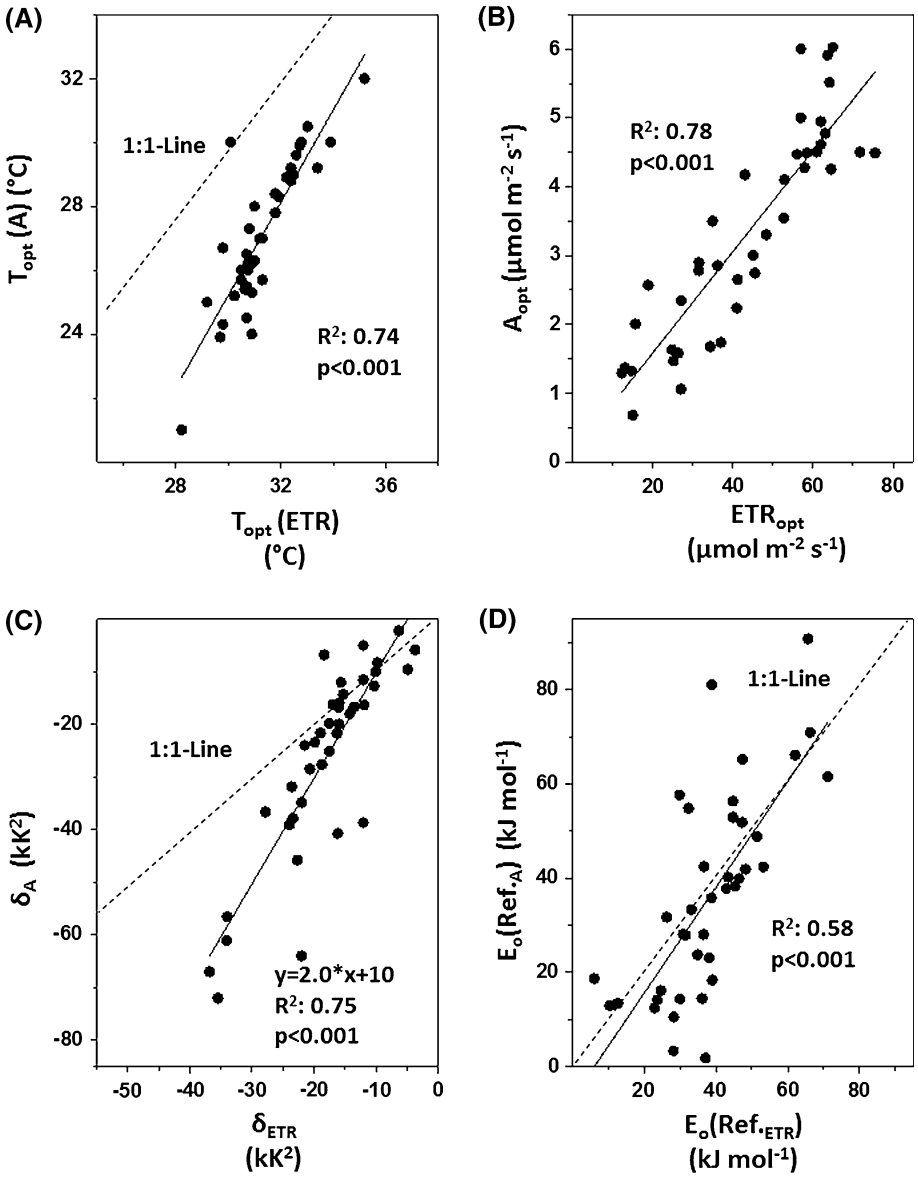

Fig. 5 Relationships between parameters of temperature-dependent photosynthesis and electron transport in the second set of experiments. **a** Correlation between optimum temperatures of photosynthesis and electron transport. **b** Correlation between peak rates of photosynthesis and electron transport achieved at their respective optimum temperature. **c** Correlation between the temperature sensitivity of E_{oA} (=δ_A) and that of E_{oETR} (=δ_{ETR}). **d** Correlation between the activation energy of A at the reference temperature ($E_o(Ref_A)$) and that of electron transport at the reference temperature ($E_o(Ref_{ETR})$)

Discussion

The present study corroborates findings by June et al. (2004) that instantaneous, temperature-dependent rates of thylakoid electron transport (J or ETR) are symmetrical around the optimum temperature. In formal descriptions of this phenomenon, electron transport at the thermal optimum (i.e., $J(T_o)$) and T_o are set as variables (see Eq. 3). For many species, the optimum temperature (T_o) is quite versatile and varies with changing growth temperature (Berry and Björkman 1980; Mawson and Cummins 1989; Yamasaki et al. 2002; Yamori et al. 2008; see Fig. 6).

In the present study, we used a modified Arrhenius equation with T_{ref} as fixed parameter, in order to characterize temperature-dependent electron transport in response to different light intensity (sensu Eq. 1). Increasing light intensity did not affect T_{opt} of ETR, but caused a clear hyperbolic increase in ETR_{opt} (see also Thornley and Johnson 1990). Below T_{opt}, increasing light intensity generally resulted in steep increases in ETR, which then equally rapidly declined above T_{opt} (compare Fig. 6), but this effect varied between leaves. Surprisingly, the parameters $E_o(Ref_{ETR})$ and δ_{ETR} were strongly correlated ($R^2 = 0.95$, Fig. 2d). This correlation was derived from 38 independent temperature curves of different leaves, suggesting common mechanism(s) regulate thylakoid electron transport—despite large variation in response to contrasting light intensity (Fig. 2e).

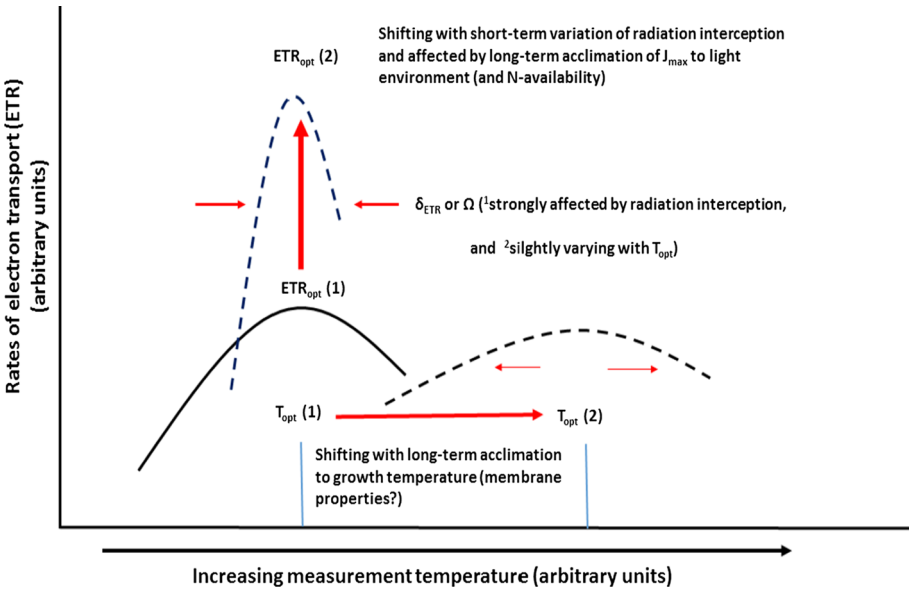

Fig. 6 Flexibility of temperature-dependent thylakoid electron transport. T_{opt} of electron transport acclimates to long-term variation of growth temperature, whereas δ_{ETR} and ETR_{opt} are more prone to short-term variation of light interception. For demonstrational purposes, the breadth of symmetric responses is exaggerated. [1]Results of the present study; [2]Results from a literature survey by June et al. (2004)

A mechanistic basis for correlation of $E_o(Ref_{ETR})$ with δ_{ETR} and symmetry of temperature-dependent electron transport: thermodynamic and general considerations

Many studies from diverse disciplines have reported a phenomenon known as the 'compensation effect' (Liu and Guo 2000). This effect relates to observations that the enthalpy of activation ($\Delta H^{\ddagger}$) is frequently correlated with the entropy of activation ($\Delta S^{\ddagger}$) of a series of connected chemical reactions (Liu and Guo 2000). Might this effect also be responsible for the close correlation between $E_o(Ref_{ETR})$ and δ_{ETR}?

For the most part, chemical reactions not catalyzed by enzymes obey classical Arrhenius kinetics and can be characterized by linear plots of ln k versus $1/T$, where the rate constant, k, is given by:

$$k = Be^{-\frac{E_a}{\Re T}} \tag{8}$$

Developing his 'transition state theory' of absolute reaction kinetics, Eyring (1935) showed that the activation barrier (E_a) to a reaction is equivalent to the free energy change of activation ($\Delta G^{\ddagger}$). From the thermodynamic relation $\Delta G^{\ddagger} = \Delta H^{\ddagger} - T\Delta S^{\ddagger}$, Eyring derived the following expression:

$$k = \frac{k_B T \times \kappa}{h} \times e^{\left(\Delta S^{\ddagger}/\Re\right)} e^{-\left(\Delta H^{\ddagger}/\Re T\right)}, \tag{9}$$

where k_B is the Boltzmann constant, h is the Planck constant, and κ is a 'transmission coefficient'. The term $\frac{k_B T \times \kappa}{h} \times e^{\left(\Delta S^{\ddagger}/\Re\right)}$ corresponds to the pre-exponential factor B of the original Arrhenius equation. Possible relations between $\Delta H^{\ddagger}$ and $\Delta S^{\ddagger}$ have no effect on the *exponent* of temperature-dependent reaction rates, and cannot account for the correlation between $E_o(Ref_{ETR})$ and δ_{ETR} (both appearing as temperature-dependent variables in the exponent of the modified Arrhenius equation; see Eq. 1 and Kruse et al. 2011, 2016).

For most enzyme-catalyzed reactions, curved plots of ln k versus 1/T are the rule, rather than the exception (i..e Sturtevant and Mateo 1978; Silvius and McElhaney 1980). Under in vitro conditions, this curvature can satisfactorily be explained by $C_p^{\ddagger} \neq 0$ (where $C_p^{\ddagger}$ is the heat capacity of activation at constant pressure), owing to the many and complex intramolecular interactions and rotational and vibrational degrees of freedom in enzyme molecules (Silvius and McElhaney 1981). Ma et al. (2000) introduced the concept of a 'transition state ensemble' in enzyme catalysis. Their model assumes a broad range of activated conformations, rather than just one, well-defined structure.

In planta, temperature-related activation, or deactivation, of allosteric enzymes add another level of complexity (Han 1972; Silvius and McElhaney 1981). Furthermore, for any chain of interdependent reactions (like thylakoid electron flow), the different kinetic properties of involved components may change the rate-limiting step(s) as leaf temperature increases. Theoretical analysis of comparatively 'simple' model systems, assuming different apparent activation energies of just two enzyme-catalyzed reactions, predicts a smooth transition curvature that links two linear asymptotes in Arrhenius plots (Han 1972). More than two reactions results in complex interactions; not easily described mathematically. While thermodynamic and

kinetic factors contribute to non-linearity in Arrhenius plots (Hulett 1964), such models cannot easily account for an apparent lack of inflection points, or for the symmetry of temperature-dependent thylakoid electron transport *in planta* (Han 1972; Silvius and McElhaney 1981; Kubo 1985).

A classic example is that using isolated chloroplasts and measuring O_2 release in the presence of saturating K_3-$[Fe(CN)_6]$ as electron acceptor (Mitchell and Barber 1986), suggests full-chain uncoupled electron transport that accords with a linear, Arrhenius description for temperature dependency. Using intact leaves on the other hand (Mitchell and Barber 1986), produces curvature in Arrhenius plots of photosynthetic O_2 evolution.

Steady-state electron flow *in planta*: 'Limitation' or 'Coordination'?

Electron transfer between most reactants in transfer chains involves spatially fixed and oriented sites, in close proximity to one another (Marcus and Sutin 1985). Electron transfer between different redox couples of PSII and PSI is rapid (timescales between 10^{-11} and 10^{-4} s) and largely independent of temperature (Malkin and Niyogi 2000). Electron transfer reactions involving the mobile electron carrier plastoquinone, are one or two orders of magnitude slower. In particular, oxidation of reduced plastoquinone (PQH_2) via the Cyt-b_6f complex is a bottleneck in thylakoid electron transport, taking about 10–20 ms and seemingly 'limits' whole-chain electron transport irrespective of incubation temperature (Haehnel 1984; Ott et al. 1999; Malkin and Niyogi 2000).

At a macroscopic scale (i.e., entire chloroplasts), frequencies of interaction between PQH_2 molecules and *populations* of Cyt-b_6f complexes are subject to physiological regulation. For example, exposure to cold triggers changes in membrane viscosity, either via changes of fatty acid composition (Raison et al. 1980; Barber et al. 1984; Mitchell and Barber 1986), or via increases in protein/lipid ratios of thylakoids (in particular increased expression of Cyt-b_6f; Yamori et al. 2005). These long-term, acclimatory responses help shift the T_{opt} of ETR. In the short term, the oxidation state of the plastochinone pool (PQH_2/PQ) adjusts swiftly to metabolic requirements via cyclic electron transport around PSI (Moss and Bendall 1984), which varies with light intensity (Laisk et al. 2005). The close correlation between $E_o(\mathrm{Ref_{ETR}})$ and δ_{ETR}, and the constant temperature sensitivity of E_{oETR}, suggest a highly regulated process.

Respiration studies provide clues to the nature of regulation of PQH_2/PQ under steady-state conditions. The temperature response of mitochondrial O_2 reduction (R_{O2}) can be described by analogy with Eq. 1, with equally strong correlation between the two exponent variables (Kruse et al. 2011, 2012; also see Supplementary Information Figure S1A). Inhibition of cytochrome oxidase (COX) by application of CN^- changes the downward curvature (concave) of modified Arrhenius plots, to convex upwards (i.e., δ_{RO2} became positive). Conversely, inhibition of alternative oxidase enforces electron flux through the cytochrome pathway and results in more negative δ_{RO2}, coupled to concomitant changes of $E_o(\mathrm{Ref_{RO2}})$ in the opposite direction (Kruse et al. 2011). Linearity of relations between $E_o(\mathrm{Ref_{RO2}})$ and δ_{RO2}, suggests that terminal oxidase activities are tightly co-ordinated and mutually interdependent. In an evolutionary sense, this helps optimize and match ATP synthesis and production of TCA cycle intermediates to cellular demand (see Kruse et al. 2011, compare Fig. 7a).

In functional terms, cyclic electron flow around PSI (CEF) shares many similarities with the alternative path of mitochondrial electron flow. CEF helps adjust ATP/NADPH production ratios to metabolic requirements (Fig. 7b). Ferredoxin-plastoquinone reductase (FQR), and its physiological role in vivo, has long been a matter of debate (Heber et al. 1995; Munekage et al. 2004; DalCorso et al. 2008). In a recent development, Hertle et al. (2013) have shown that antimycin A-sensitive PGRL1 has similar characteristics to FQR. Notably, thioredoxins (TRXs) promote formation of PGRL1 monomers, which is a possible mechanism for modulating activity of FQR in a fashion similar to that of AOX. The exact physiological role of CEF *in planta* remains controversial because we currently lack the ability to measure CEF directly (Shikanai 2007; Johnson 2011).

We suggest that the temperature dependency of Φ_{PSII} is a simple, albeit indirect, means to estimate CEF under steady-state conditions, and that low (more negative) δ_{ETR} values are *indicative* for high rates of CEF under high light. This suggestion is supported by findings of Joliot and Joliot (2006), showing that under steady-state illumination the contribution of cyclic electron flow to PSI turnover increases as a function of light intensity (from 0 % under weak light to 50 % under saturating light; Joliot and Joliot 2006).

It is not possible to identify a single process that 'limits' electron flow under steady-state conditions, because electron source activity (i.e., Φ_{PSII}) is subject to subtle feedback regulation via electron sink activity (i.e., Ferredoxin-NADP Reductase activity, Fig. 7b)—mediated by pH. For example, enhanced protonation of chlorophyll proteins in thylakoid lumens, facilitates binding to zeaxanthin, associated with conformational changes that convert these proteins into energy-dissipating traps (non-photochemical quenching; Heber and Walker 1992; Horton et al. 1996; Johnson 2011). Consequently, Φ_{PSII} (at T_{opt}) slows as light

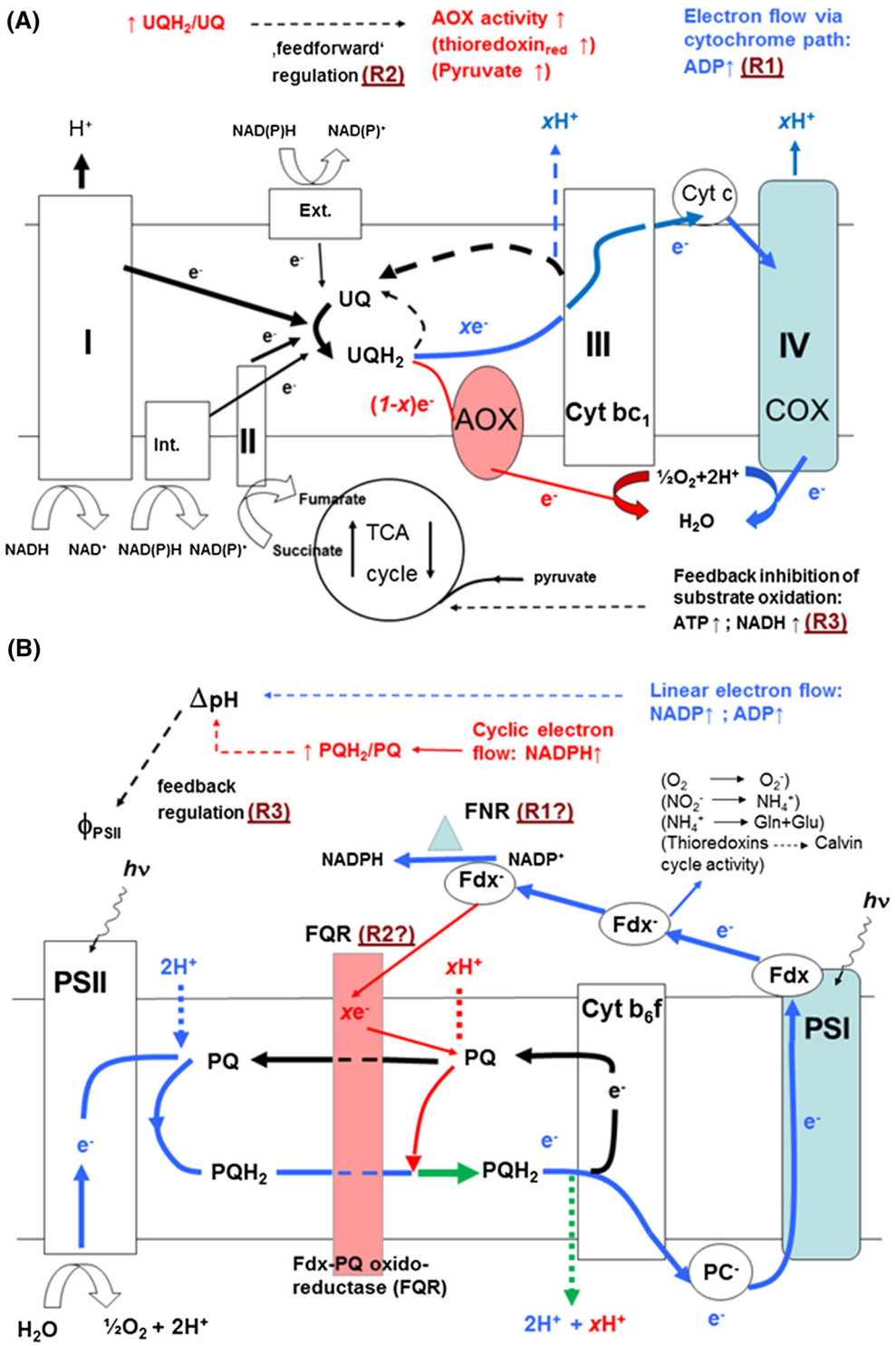
(A)
↑ UQH2/UQ
‚feedforward' regulation (R2)
AOX activity ↑ (thioredoxinred ↑) (Pyruvate ↑)
Electron flow via cytochrome path: ADP↑ (R1)
H+
NAD(P)H
NAD(P)+
xH+
xH+
Ext.
Cyt c
e-
UQ
UQH2
xe-
I
III
IV
Int.
II
(1-x)e-
AOX
Cyt bc1
COX
½O2+2H+
H2O
Fumarate
Succinate
TCA cycle
NADH
NAD+
NAD(P)H
NAD(P)+
pyruvate
Feedback inhibition of substrate oxidation: ATP↑ ; NADH ↑ (R3)
(B)
ΔpH
Linear electron flow: NADP↑ ; ADP↑
↑ PQH2/PQ
Cyclic electron flow: NADPH↑
feedback regulation (R3)
ϕPSII
(O2 → O2-)
(NO2- → NH4+)
(NH4+ → Gln+Glu)
(Thioredoxins ----▸ Calvin cycle activity)
FNR (R1?)
NADPH
NADP+
hν
Fdx-
FQR (R2?)
Fdx
PSII
2H+
xH+
xe-
Cyt b6f
PSI
PQ
PQH2
PC-
Fdx-PQ oxido-reductase (FQR)
H2O
½O2 + 2H+
2H+ + xH+

◀**Fig. 7** Principal regulatory features of electron flow in mitochondrial and thylakoid membranes, accounting for variation in the shape of temperature-dependent electron flow—as defined by δ_{RO2} for mitochondrial electron flux in the dark or δ_{ETR} for thylakoid electron flux in the light. It is suggested that the δ parameter reflects a distinct flux mode (see "Discussion" section). **a** In mitochondria, electron flow via the cytochrome path is chiefly regulated by cellular ATP demand. Over-reduction of the ubiquinol pool can cause activation of alternative oxidase, in order to (i) prevent formation of ROS and (ii) keep the TCA cycle operative (under low ADP availability) for continued production of intermediates for anabolism (i.e., *de novo* synthesis of amino acid). Enhanced contribution of AOX to mitochondrial electron flux causes δ_{RO2} to become more positive (Kruse et al. 2011). **b** In chloroplasts, rates of linear electron flow are chiefly governed by rates of ATP and NADPH consumption in the Calvin cycle. Depending on light intensity (and other influences), metabolic demand for ATP changes relative to that for NADPH. Cyclic electron flow around PS I (CEF) apparently helps regulate different requirements for ATP/NADPH, presumably via FNR and/or FQR. Enhanced activity of FQR apparently causes δ_{ETR} to become more negative. We also suggest that the temperature dependencies of electron flow and CO_2 assimilation (i.e., δ_{ETR} and δ_A) remain tightly co-ordinated via the thioredoxin system (target enzymes: Carbonic anhydrase, Rubisco activase, Glyceraldehyde-3P-dehydrogenase, Fructose-1,6-P_2-phosphatase, Sedoheptulose-1,7-P_2-phosphatase, Ribulose-5P-kinase; Buchanan and Balmer 2005). Note that, *in planta*, FQR is loosely associated with PSI. That is, Fig. 7b is an oversimplification, because there exists distinct PQ pools within appressed and non-appressed regions of thylakoid membranes, respectively ('lateral heterogeneity'). For demonstrational purposes, we assumed one PQ pool, receiving electrons from PSII and FQR. Abbreviations: *Figure A* AOX, alternative oxidase; COX, cytochrome oxidase. R1–R3: Central points for feedback regulation of mitochondrial electron transport. *Figure B* FNR, Ferredoxin-NADP oxidoreductase; FQR, Ferredoxin-PQ oxidoreductase (=PGRL1, Hertle et al. 2013); ΔpH; transmembrane proton gradient; R1–R3: Central points for putative feedback regulation of thylakoid electron transport. Cyclic and linear pathways compete for re-oxidation of ferredoxin that freely diffuses in the stroma (Joliot and Joliot 2006). Given that FNR (i.e., Lehtimäki et al. 2014) and FQR (Hertle et al. 2013) are subject to post-translational modification, the partitioning of electrons between the two pathways may be highly regulated. Note that Fig. 7 does not claim to be stochiometrically correct. Rather, the factors x or $(1 - x)$ indicate the partitioning of electrons between different pathways

intensity increases (Fig. 1d). Cyclic electron transport around PSI is also coupled to vectorial proton transfer, and the contribution of CEF to ΔpH becomes apparent in temperature dependency of Φ_{PSII}. Operation of CEF significantly affects the P/O ratio of entire chloroplasts or leaves. It seems useful to note that where any given δ_{ETR} falls between $E_o(Ref_{ETR})$ and δ_{ETR}, it indicates the balance between PSII source activity and ATP synthesis under steady-state conditions. Electron flow through the alternative pathway decreases P/O, whereas operation of cyclic electron flow around PSI increases P/O. δ_{RO2} values are frequently positive (Supplementary Information Fig.S1A), whereas δ_{ETR} values are always negative (Fig. 2f). As a result, temperature responses of respiratory O_2 uptake or CO_2 evolution largely remain exponential, but those of photosynthetic CO_2 uptake appear parabolic, with variable breadth.

Relation between flux mode of thylakoid electron flow and Calvin cycle activity

The symmetry of *A*/*T* curves depended on light intensity (Fig. 2h). A_{opt} increased hyperbolically, while δ_A decreased linearly with light. Similar results were obtained by Ludlow and Wilson (1971; Fig. 3 in the review by Berry and Björkmann 1980) and Oberhuber and Edwards (1993) but these early studies have not been widely replicated. Early simulations of *A*/*T* responses under saturating light, assuming known temperature effects on the specificity factor of Rubisco, rate-saturating RuP_2 supply to the enzyme, and constant stomatal conductance (Berry and Björkmann 1980), showed an increasing mismatch between simulated and observed net CO_2 assimilation at leaf temperatures above 20 °C.

The most widely adopted (and cited) explanation for this mismatch is limited capacity for RuP_2 regeneration, which becomes particularly problematic as temperature increases (Berry and Björkmann 1980; Harley et al. 1985).

Results of the present study suggest an alternative interpretation, namely that steady-state rates of CO_2 assimilation remain tightly co-ordinated with those of thylakoid electron transport, whereby the mode of electron flow (linear versus cyclic electron flow) is regulated by metabolic requirements for ATP relative to those for NADPH. For example, if rates of CO_2 assimilation exceed rates of cytosolic sucrose synthesis and export under high light intensity, additional ATP is required for starch synthesis in chloroplasts. Further, 'excess' reducing equivalents under high illumination can be exported from chloroplasts via the malate/oxalacetate shuttle, in order to power processes other than Calvin cycle activity (Yoshida et al. 2007). It remains true to state that we have limited understanding on how chloroplast metabolism is integrated with other cellular processes (Raghavendra and Padmasree 2003; Johnson 2011).

In the present study δ_{ETR} and δ_A were tightly related (Fig. 5c), but light intensity had additional influences on δ_A (Fig. 4d). With increasing illumination, enhanced operation of CEF increases the ATP/NADPH production ratio above that needed for steady-state CO_2 fixation in the Calvin cycle (i.e., ATP/NADPH >1.5; Buchanan et al. 2000). It is very arguable that the 'speed' of turnover of ATP, relative to that of NADPH, regulates the mode of thylakoid electron transport (Fig. 7b; Endo et al. 2005; Hald et al. 2008). The constancy of δ_{ETR} (and δ_A) implies that the ratio of these rates of turnover is (mostly) independent of incubation temperature.

A/*T* curves remained symmetrical irrespective of applied c_a. Further, temperature sensitivity of E_{oA} (or δ_A) did not change with incubation temperature (Fig. 1c), as might have been expected at least for measurements at $c_a <$ ambient. Symmetry of *A*/*T* curves leads to a conclusion that the ratio of $RubP_2$ carboxylation:oxygenation does not change with incubation temperature. There is evidence that temperature-induced changes in kinetic properties of Rubisco, such as favoring the oxygenation reaction at greater *T*, are compensated by increased stomatal conductance (Sage 2013), or increased mesophyll conductance to CO_2 transfer (von Caemmerer and Evans 2015). The close-to-instantaneous responses of mesophyll conductance to greater leaf temperature point to control via enzymatic processes (e.g., regulation of aquaporins, Flexas and Diaz-Espejo 2015).

Finally, the lack of temperature effects on the symmetry of *A*/*T* curves at ambient c_a, did not preclude c_a from affecting δ_A at concentrations < ambient. We observed that substomatal [CO_2] (i.e., c_i at T_{opt}) significantly influenced the correlation between $E_o(\text{Ref}_A)$ and δ_A, where δ_A declined with decreasing c_i (from -45 kK^2 at 250 µmol mol^{-1} to -60 kK^2 at 50 µmol mol^{-1}, Fig. 3e, f). Low CO_2 availability promotes CEF and is a possible explanation for this observation (Heber and Walker 1992; Heber 2002; Joliot and Joliot 2006).

Conclusions

Previously, a modified Arrhenius equation has been reported for the characterization of temperature dependency of mitochondrial electron flow (Kruse et al. 2011), and CO_2 evolution in the dark (Noguchi et al. 2015; Kruse et al. 2012, 2016). In the present study we show that this equation can also be applied for the characterization of thylakoid electron flow, which remains tightly co-ordinated with CO_2 assimilation in the light. Within the range of temperatures that do not cause irreversible damage to the photosynthetic machinery, *A*/*T* curves remain symmetrical irrespective of light intensity or substomatal [CO_2]. Enhanced illumination and low c_i have opposite effects on A_{opt}, but both factors result in *A*/*T* curves narrowing around T_{opt} (i.e., δ_A declines). The latter effect has measurable influences on the generally strong correlation between $E_o(\text{Ref}_A)$ and δ_A, affecting its slope and/or the intercept. Under steady-state conditions, δ_A is tightly related to δ_{ETR}. Variation in δ_{ETR} is most likely linked to variable contributions of cyclic versus linear electron flow, as determined by anabolic demand for ATP relative to NADPH. Previous attempts to interpret *A*/*T* responses centered around 'supply-driven' control of net photosynthesis, assuming carboxylation rates, at any given biochemical capacity (i.e., RubisCO abundance), are limited by temperature-dependent supply of substrates (either RuP_2 or CO_2 versus O_2) to the sites of carboxylation. The results of the present and a previous study (Kruse et al. 2016) rather indicate 'demand-driven' control of photosynthesis, linking different requirements for ATP and NADPH during carbon fixation to different modes of triosephosphate utilization (i.e., synthesis of starch, versus export of sucrose or amino acids). Hence, the shape of *A*/*T* curves, as defined by the δ_A parameter, can be viewed as an emergent property of whole-leaf photosynthesis, depending on the *mode* of thylakoid electron flux. Following this rationale, the peak of *A*/*T* curves, as defined by A_{opt}, would depend on the *rate* of triosephosphate utilization, with an upper limit set either by the rate of growth, or by J_{max} (and/or V_{cmax}) under prevailing resource availability or environmental conditions.

Acknowledgments The research of this study was funded by the King Saud University, Saudi Arabia (PRG-1436-24), and the University of Sydney, Australia.

References

Baker NR, Harbinson J, Kramer (2007) Determining the limitations and regulations of photosynthetic energy transduction in leaves. Plant Cell Environ 30:107–125

Barber J, Ford RC, Mitchell RAC, Millner PA (1984) Chloroplast thylakoid membrane fluidity and its sensitivity to temperature. Planta 161:375–380

Battaglia M, Beadle C, Loughhead S (1996) Photosynthesis temperature response of *Eucalyptus globulus* and *Eucalyptus nitens*. Tree Physiol 16:81–89

Berry JA, Björkman O (1980) Photosynthetic response and adaptation to temperature in higher plants. Annu Rev Plant Physiol 31:491–543

Buchanan BB, Balmer (2005) Redox regulation: a broadening horizon. Annu Rev Plant Biol 56:187–220

Buchanan BB, Gruissem W, Jones RL (2000) Biochemistry and molecular biology of plants. American Society of Plant Physiologists, Rockville, MD

Clarke JE, Johnson GN (2001) In vivo temperature dependence of cyclic and pseudocyclic electron transport in barley. Planta 212:808–816

DalCorso G, Pesaresi P, Masiero S, Aseeva E, Schünemann D, Finazzi G, Joliot P, Barbato R, Leister D (2008) A complex containing PGRL1 and PGR5 is involved in the switch between linear and cyclic electron flow in *Arabidopsis*. Cell 132:273–285

Endo T, Kawase D, Sato F (2005) Stromal over-reduction by high-light stress as measured by decreases in P700 oxidation by far-red light and its physiological relevance. Plant Cell Physiol 46:775–781

Eyring H (1935) The activated complex and the absolute rate of chemical reactions. Chem Rev 17:65–77

Farquhar GD, von Caemmerer S, Berry JA (1980) A biochemical model of photosynthetic CO_2 assimilation in leaves of C_3 species. Planta 149:78–90

Flexas J, Diaz-Espejo A (2015) Interspecific differences in temperature response of mesophyll conductance: food for thought on its origin and regulation. Plant Cell Environ 38:625–628

Genty B, Briantais J-M, Baker NR (1989) The relationship between quantum yield of photosynthetic electron transport and quenching of chlorophyll fluorescence. Biochim Biophys Acta 990:87–92

Gunderson CA, O'Hara KH, Campion CM, Walker AW, Edwards NT (2010) Thermal plasticity of photosynthesis: the role of acclimation in forest responses to a warming climate. Glob Change Biol 16:2272–2286

Haehnel W (1984) Photosynthetic electron transport in higher plants. Annu Rev Plant Physiol Plant Mol Biol 35:659–693

Hald S, Nandha B, Gallois P, Johnson GN (2008) Feedback regulation of photosynthetic electron transport by NADP(H) redox poise. Biochim Biophys Acta 1777:433–440

Han MH (1972) Non-linear Arrhenius plots in temperature-dependent kinetic studies of enzyme reactions. I. Single transition processes. J Theor Biol 35:543–568

Harley PC, Weber JA, Gates (1985) Interactive effects of light, leaf temperature, CO_2 and O_2 on photosynthesis in soybean. Planta 165:249–263

Heber U (2002) Irrungen, Wirrungen? The Mehler reaction in relation to cyclic electron transport in C_3 plants. Photosynth Res 73:223–231

Heber U, Walker D (1992) Concerning a dual function of coupled cyclic electron-transport in leaves. Plant Physiol 100:1621–1626

Heber U, Gerst U, Krieger A, Neimanis S, Kobayashi Y (1995) Coupled cyclic electron transport in intact chloroplasts and leaves of C_3 plants: does it exist? If so, what is its function? Photosynth Res 46:269–275

Hertle AP, Blunder T, Wunder T, Pesaresi P, Pribil M, Armbruster U, Leister D (2013) PGRL 1 is the elusive ferredoxin-plastoquinone-reductase in photosynthetic cyclic electron flow. Mol Cell 49:511–523

Horton P, Ruban RG, Walters RG (1996) Regulation of light harvesting in green plants. Annu Rev Plant Physiol Plant Mol Biol 47:655–684

Hulett JR (1964) Deviations from the Arrhenius equation. Quart Rev 3:227–242

Hüve K, Bichele I, Rasulov B, Niinemets Ü (2011) When it is too hot for photosynthesis: heat-induced instability of photosynthesis in relation to respiratory burst, cell permeability changes and H_2O_2 formation. Plant Cell Environ 34:113–126

Johnson GN (2011) Physiology of PSI cyclic electron transport in higher plants. Biochim Biophys Acta 1807:384–389

Joliot P, Joliot A (2006) Cyclic electron flow in C_3 plants. Biochim Biophys Acta 1757:362–368

June T, Evans JR, Farquhar GD (2004) A simple new equation for the reversible temperature dependence of photosynthetic electron transport: a study on soybean leaf. Funct Plant Biol 31:275–283

Kruse J, Rennenberg H, Adams MA (2011) Steps towards a mechanistic understanding of respiratory temperature responses. New Phytol 189:659–677

Kruse J, Turnbull T, Adams MA (2012) Disentangling respiratory acclimation and adaptation to growth temperature by *Eucalyptus* spp. New Phytol 195:149–163

Kruse J, Adams MA, Kadinov G, Arab L, Kreuzwieser J, Alfarraj S, Schulze W, Rennenberg H (2016) Characterization of photosynthetic acclimation in *Phoenix dactylifera* by a modified Arrhenius equation originally developed for leaf respiration. Photosyn Res (re-submitted)

Kubo K (1985) A view on the break in the Arrhenius plot. J Theor Biol 115:551–569

Laisk A, Eichelmann H, Oja V, Peterson RB (2005) Control of cytochrome *b(6)f* at low and high light intensity and the cyclic electron transport in leaves. Biochim Biopys Acta 1708:79–90

Lehtimäki N, Koskela MM, Dahlström KM, Pakula E, Lintala M, Scholz M, Hippler M, Hanke GT, Rokka A, Battchikova N, Salminen TA, Mulo P (2014) Posttranslational modifications of Ferredoxin-$NADP^+$ oxidoreductase in Arabidopsis chloroplasts. Plant Physiol 166:1764–1776

Lin Y-S, Medlyn BE, Ellsworth DS (2012) Temperature responses of leaf net photosynthesis: the role of component processes. Tree Physiol 32:219–231

Liu L, Guo Q-X (2000) Isokinetic relationship, isoequilibrium relationship, and enthalpy-entropy compensation. Chem Rev 101:673–695

Ludlow MM, Wilson GL (1971) Photosynthesis of tropical pasture plants. I. Illuminance, carbon dioxide concentration, leaf temperature, and leaf-air vapor pressure difference. Aust J Biol Sci 24:449–470

Ma B, Kumar S, Tsai C-J, Hu Z, Nussinov R (2000) Transition-state ensemble in enzyme catalysis: possibility, reality, or necessity? J Theor Biol 203:383–397

Malkin R, Niyogi K (2000) Photosynthesis. In: Buchanan BB, Gruissem W, Jones RL (ed) Biochemistry and molecular biology of plants, pp 508–566

Marcus RA, Sutin N (1985) Electron transfers in chemistry and biology. Biochim Biophys Acta 811:265–322

Mawson BT, Cummins WR (1989) Thermal acclimation of photosynthetic electron transport activity by thylakoids of Saxifraga cernua. Plant Physiol 89:325–332

Medlyn BE, Dreyer E, Ellsworth D, Harley PC, Kirschbaum MUF, Le Roux X, Montpied P, Strassmeyer J, Walcroft A, Wang K, Loustau D (2002) Temperature response of parameters of a biochemically based model of photosynthesis. II. A review of experimental data. Plant Cell Environ 25:1167–1179

Mitchell RAC, Barber J (1986) Adaptation of photosynthetic electron-transport rate to growth temperature in pea. Planta 169:429–436

Moss DA, Bendall DS (1984) Cyclic electron transport in chloroplasts. The Q-cycle and the site of action of antimycin. Biochim Biophys Acta 767:389–395

Munekage Y, Hashimoto M, Miyake C, Tomizawa K, Endo T, Tasaka M, Shikanai T (2004) Cyclic electron transport around photosystem I is essential for photosynthesis. Nature 429:579–582

Niinemets Ü, Oja V, Kull O (1999) Shape of leaf photosynthetic electron transport versus temperature response curve is not constant along canopy light gradients in temperate deciduous trees. Plant Cell Environ 22:1497–1514

Noguchi K, Yamori W, Hikosaka K, Terashima I (2015) Homeostasis of the temperature sensitivity of respiration over a range of growth temperatures indicated by a modified Arrhenius model. New Phytol. doi:10.1111/nph.13339

Oberhuber W, Edwards GE (1993) Temperature dependence of the linkage of quantum yield of photosystem II to CO_2 fixation in C_4 and C_3 plants. Plant Physiol 101:507–512

Ott T, Clarke J, Birks K, Johnson G (1999) Regulation of the photosynthetic electron transport chain. Planta 209:250–258

Raghavendra AS, Padmasree K (2003) Beneficial interactions of mitochondrial metabolism with photosynthetic carbon assimilation. Trends Plant Sci 8:546–553

Raison JK, Berry JA, Armond PA, Pike CS (1980) Membrane properties in relation to the adaptation of plants to temperature stress. In: Turner NC, Kramer PJ (eds) Adaptation of plants to water and high temperature stress. Wiley, New York, pp 261–273

Sage RF (2013) Photorespiratory compensation: a driver for biological diversity. Plant Biol 15:624–638

Schreiber U (2004) Pulse-amplitude-modulation (PAM) fluorometry and saturation pulse method: an overview. Adv Photosyn Respir 19:279–319

Seemann JR, Berry JA, Downton WJS (1984) Photosynthetic response and adaptation to high temperature in desert plants. Plant Physiol 75:364–368

Shikanai T (2007) Cyclic electron transport around photosystem I: genetic approaches. Annu Rev Plant Biol 58:199–217

Siedow JA, Day DA (2000) Respiration and photorespiration. In: Buchanan BB, Gruissem W, Jones RL (eds) Biochemistry and molecular biology of plants. American Society of Plant Physiologists, Rockville, pp 676–728

Silvius JR, McElhaney RN (1980) Membrane lipid physical state and modulation of the Na^+, Mg^{2+}-ATPase activity in *Acholeplasma laidlawii* B. Proc Natl Acad Sci USA 77:1255–1259

Silvius JR, McElhaney RN (1981) Non-linear Arrhenius plots and the analysis of reaction and motional rates in biological membranes. J Theor Biol 88:135–152

Smith NG, Dukes JS (2013) Plant respiration and photosynthesis in global-scale models: incorporating acclimation to temperature and CO_2. Glob Change Biol 15:308–314

Sturtevant JM, Mateo PL (1978) Proposed temperature-dependent conformational transition in D-amino acid oxidase: a differential scanning microcalorimetric study. Proc Natl Acad Sci USA 75:2584–2587

Tenhunen JD, Yocum CS, Gates DM (1976) Development of a photosynthesis model with an emphasis on ecological applications. I. Theory. Oecologia 26:89–100

Thornley JHM, Johnson RL (1990) Plant and crop modeling. A mathematical approach to plant and crop physiology. Oxford Science Publications, Oxford

von Caemmerer S, Evans JR (2015) Temperature responses of mesophyll conductance differ greatly between species. Plant Cell Environ 38:629–637

Way DA, Yamori W (2014) Thermal acclimation of photosynthesis: on the importance of adjusting our definitions and accounting for thermal acclimation of respiration. Photosynth Res 119:89–100

Yamasaki T, Yamakawa T, Yamane Y, Koike H, Satoh K, Katoh S (2002) Temperature acclimation of photosynthesis and related changes in photosystem II electron transport in winter wheat. Plant Physiol 128:1087–1097

Yamori W, Noguchi K, Terashima I (2005) Temperature acclimation of photosynthesis in spinach leaves: analysis of photosynthetic components and temperature dependencies of photosynthetic partial reactions. Plant Cell Environ 28:536–547

Yamori W, Noguchi K, Kashino Y, Terashima I (2008) The role of electron transport in determining the temperature dependence of the photosynthetic rate in spinach leaves grown at contrasting temperatures. Plant Cell Physiol 49:583–591

Yoshida K, Terashima I, Noguchi K (2007) Up-regulation of mitochondrial alternative oxidase concomitant with chloroplast over-reduction by excess light. Plant Cell Physiology 48: 606–614

Zhang R, Sharkey TD (2009) Photosynthetic electron transport and proton flux under moderate heat stress. Photosynth Res 100: 29–43